


*17th World Conference on Earthquake Engineering, 17WCEE*
*Sendai, Japan - September 13th to 18th 2020*

# A NOVEL SMA-CABLE-BASED PURE FRICTION SLIDING BEARING FOR SEISMIC RESILIENT IMPROVEMENT OF HIGHWAY BRIDGES

D. Liang[(1)], Y. Zheng[(2)], C. Fang[(3)]

[(1)] *Graduate student, Department of Structural Engineering, Tongji University, Shanghai 200092, China, dong_liang@tongji.edu.cn*
[(2)] *Assistant professor, Department of Bridge Engineering, Tongji University, Shanghai 200092, China, yzheng@tongji.edu.cn*
[(3)] *Associate professor, Department of Structural Engineering, Tongji University, Shanghai 200092, China, chengfang@tongji.edu.cn*

## *Abstract*

Seismic isolation bearings have been extensively used for seismic damage mitigation of bridge structures. Conventional pure friction (PF) sliding bearing is often criticized by some problems such as excessive sliding displacement and unrecovered deformation under strong ground motions. To solve these problems, this paper proposes a new SMA-cable-based pure friction (SMA-PF) sliding bearing system which consists of a steel-Teflon sliding bearing and supplementary shape memory alloy (SMA) cables. The former is responsible for carrying the vertical loads and providing moderate energy dissipation as a result of its frictional behavior, and the latter can provide re-centering force and additional damping, and act as restrainers when the displacement is large. The SMA cables are flexibly connected to the upper and lower bearing plates by hemispherical nuts, which can achieve effective force transmission when there is relative motion in any horizontal direction between the bearing plates. The design also makes it convenient to inspect and replace the SMA cables after strong earthquakes. The working principle and mechanical performance of the conventional PF bearing system and the proposed SMA-PF bearing system are first described, and the design details of the latter are particularly highlighted. Subsequently, the basic mechanical behavior of the individual SMA cable is understood via analytical descriptions that are verified by a preliminary experimental study. It is observed that the SMA cables are able to reasonably "scale up" the fundamental properties, such as limited residual deformation and good ductility, of the SMA wires. Finally, a case study is conducted to investigate the effectiveness of the SMA-PF bearing in seismic control of prototype bridges. Three-dimensional finite-element models of the bridges are established in OpenSees software. The result shows that the SMA-PF bearing can effectively control the horizontal displacements of the girder deck compared with the conventional PF bearing, and severe damages such as the unseating or collapse are prevented. Although the introduction of the SMA cables can in some cases increase the horizontal force transferred to the piers, the inelastic deformation of the plastic hinge zone at the bottom of the piers stays at a controllable level due to the low-stiffness transformation plateau of the SMA cables.

*Keywords: shape memory alloy cables, pure friction sliding bearing, restrainer, bridge, seismic resilient, self-centering*

 



## 1. Introduction

In recent decades, isolation bearings have been extensively applied in highway bridges for seismic hazard mitigation. Pure friction (PF) sliding bearing is a representative and popular type of isolation bearing in practice [1]. These bearings aim to decouple the superstructure from the substructure and hence to shift the fundamental period away from the predominant period of earthquakes. However, the unreliability of the bearings because of their increasing flexibility was highlighted in these years (especially for simply supported bridges). A large amount of damaged or even collapsed bridges after earthquakes were attributed to excessive displacements of bearings according to post-earthquake survey reports[2]–[4]. In order to solve this problem, new seismic protection technologies such as cable/bar restrainers, dampers, and shear rod stoppers were implemented to limit the displacement of the deck [5]–[9]. As an emerging smart material, shape memory alloys (SMAs) have been considered in passive seismic control thanks to their unique superelasticity (SE) behavior[10]–[12]. SMA cables, a relatively new class of SMA elements, have been attracting increasing interests, because they combine both the advantageous properties of conventional cables and SMA[13].

This study proposes a novel type of PF sliding bearing equipped with SMA cables (SMA-PF bearing) to improve the seismic resilience of the bridges. The working principle of the new bearing is first discussed, and an experimental study on individual SMA cable specimens is then presented. This is followed by a dynamic time-history analysis on two bridge models, one with conventional PF bearings and the other one with the new SMA-PF bearings. Comparisons of the key responses such as peak displacement and pier curvature ductility are made between the two bridges, and some design comments are finally made.

## 2. System description of proposed SMA-PF sliding bearing

The newly proposed SMA-PF bearing is a combination of a basic PF sliding bearing and SMA cables. The two-dimensional and three-dimensional view of the configuration of this bearing is shown in Fig. 1. The main parts of the PF sliding bearing include a top plate, stainless steel plate, Teflon plate, middle steel plate, rubber pad, and bottom plate, all of which play an important role in sustaining normal working load. The supplemental SMA cables mainly serve as restrainers, where the size and number can be adjusted according to the practical requirement. As shown in the figure, the two ends of the SMA cables are machined into threaded bars and connected to the top and bottom plates using screw nuts with a hemispherical shape. Such a connecting mechanism enables free rotation of the cables which are mainly subjected to axial force when adapting to any horizontal displacement of the bearing.

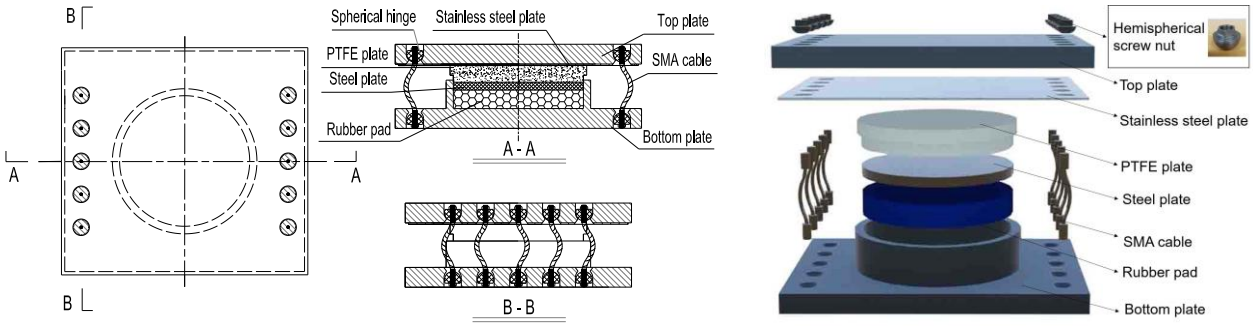


(a) (b)

**Fig. 1** Schematic illustration of SMA-PF bearing: a) two-dimension view, b) three-dimension view

Fig. 2 gives the schematic diagram of the working mechanism of the bearing at two stages, i.e. before and after the tensioning of the SMA cables. An initial slack of the SMA cables is considered to accommodate the horizontal displacement of the deck caused by shrinkage, creep, or temperature change. At this stage, the behavior of the bearing is similar to that of traditional PF sliding bearing before the tensioning of the SMA



 

cables. If the initial slack is determined, the required free length (between the rotation center of the top and bottom screw nuts) of the SMA cables could be obtained by solving Eq. (1):

$$l_f = \sqrt{l_s^2 + h^2} \tag{1}$$

where $h$ is the vertical distance between the rotation center of two screw nuts (Fig. 2(a)). The lateral load resistance ($F_{SMA\text{-}PF}$) of the bearing is only provided by the friction at this stage, as expressed by:

$$F_{SMA-PF} = \mu N \tag{2}$$

where $N$ is the vertical load applied; $\mu$ is the frictional coefficient of the contact interface.

When the relative displacement of the bearing increases until the initial slack is fully consumed, the SMA cables are tightened and start contributing to load resistance and energy dissipation (Fig.2 (b)). In this case the overall load resistance $F_{SMA\text{-}PF}$ is offered by the friction force and the horizontal component of the force provided by the SMA cables, as expressed by:

$$F_{SMA-PF} = \mu(N + F_{SMA\text{-}V}) + F_{SMA\text{-}H} \tag{3}$$

where $F_{SMA\text{-}H}$ and $F_{SMA\text{-}V}$ are the horizontal and vertical components of the axial force of SMA cables, respectively. Given the geometric features (Fig.2 (b)), $F_{SMA\text{-}H}$ and $F_{SMA\text{-}V}$ should satisfy:

$$F_{SMA\text{-}H} = \sigma_{SMA} A_{sum} \cos\theta \tag{4}$$

$$F_{SMA\text{-}V} = \sigma_{SMA} A_{sum} \sin\theta \tag{5}$$

where $\sigma_{SMA}$ is the tensile stress of the SMA cables; $A_{sum}$ is the sum of cross-sectional area of all the SMA cables functioning in the bearing system; $\theta$ is the angle between the SMA cable and the horizontal plate, as expressed by:

$$\sin\theta = \frac{h}{\sqrt{(\Delta l + l_s)^2 + h^2}} \tag{6}$$

$$\cos\theta = \frac{\Delta l + l_s}{\sqrt{(\Delta l + l_s)^2 + h^2}} \tag{7}$$

where $\Delta l$ is the further displacement of the bearing after the initial slack. While there are many hysteretic models available for describing the behavior of SMA, a widely-used flag-shaped hysteretic model with a limited number of controlling parameters is introduced here, as shown in Fig.3. Many studies have confirmed that this simplified flag-shaped model is adequate for describing the basic behavior of superelastic SMA cables. Based on this model, $\sigma_{SMA}$ could be expressed by the following set of equations:

$$\varepsilon_{SMA} = \frac{\sqrt{(\Delta l + l_s)^2 - h^2} - l_f}{l_f} \tag{8}$$

1) loading

$$\sigma_{SMA} = \varepsilon_{SMA} E_A \qquad \text{for } \varepsilon_{Ms} > \varepsilon_{SMA} > 0 \tag{9}$$

$$\sigma_{SMA} = \sigma_{Ms} + (\varepsilon_{SMA} - \varepsilon_{Ms}) k_1 E_A \quad \text{for } \varepsilon_{Mf} > \varepsilon_{SMA} > \varepsilon_{Ms} \tag{10}$$

$$\sigma_{SMA} = \sigma_{Mf} + (\varepsilon_{SMA} - \varepsilon_{Mf}) k_2 E_A \quad \text{for } \varepsilon_{Max} > \varepsilon_{SMA} > \varepsilon_{Mf} \tag{11}$$



 

2) unloading

$$\sigma_{SMA} = \sigma_{Mf} + (\varepsilon_{SMA} - \varepsilon_{Mf})k_2 E_A \quad \text{for } \varepsilon_{Max} > \varepsilon_{SMA} > \varepsilon_{Mf} \tag{12}$$

$$\sigma_{SMA} = \sigma_{Mf} - (\varepsilon_{Mf} - \varepsilon_{SMA})E_M \quad \text{for } \varepsilon_{Mf} > \varepsilon_{SMA} > \varepsilon_{As} \tag{13}$$

$$\sigma_{SMA} = \sigma_{As} - (\varepsilon_{As} - \varepsilon_{SMA})\ k_1 E_A \quad \text{for } \varepsilon_{As} > \varepsilon_{SMA} > \varepsilon_{Af} \tag{14}$$

$$\sigma_{SMA} = \varepsilon_{SMA} E_A \quad \text{for } \varepsilon_{Af} > \varepsilon_{SMA} > 0 \tag{15}$$

where $\varepsilon_{SMA}$ is the global strain of the SMA cables, which could be obtained by solving Eq. (8), and the other symbols are explained in Fig. 3.

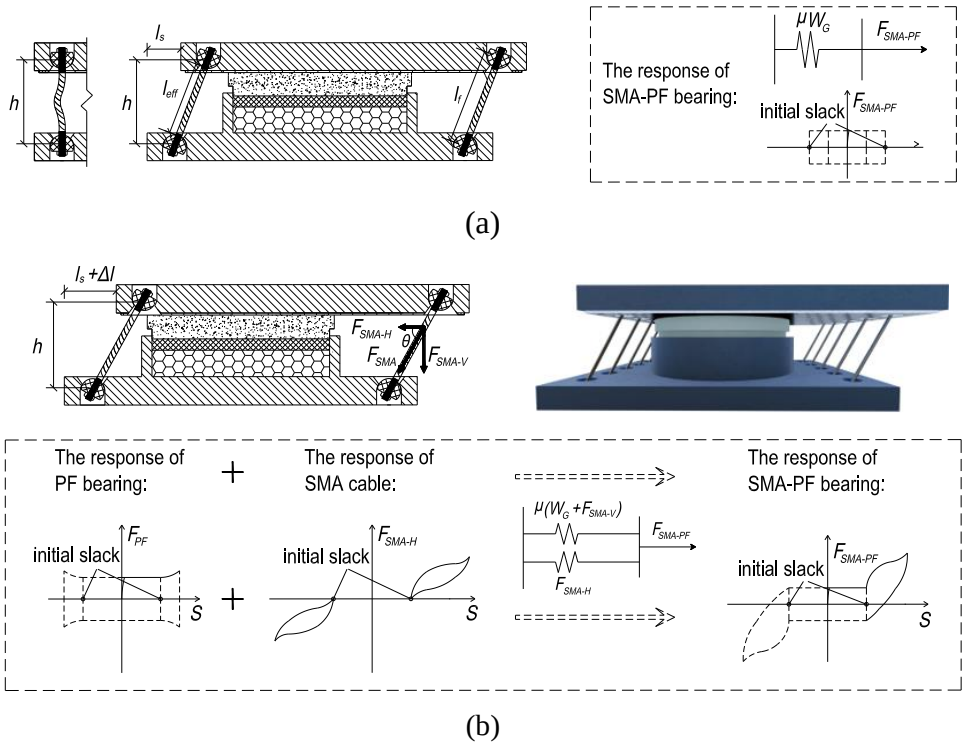


**Fig. 2** Working principles: a) before initial slack, b) after initial slack

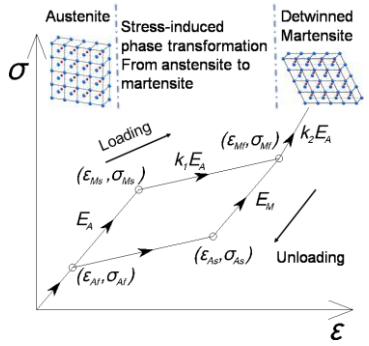


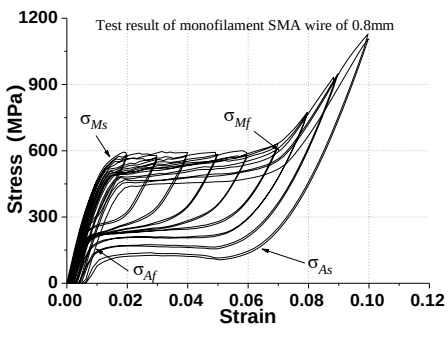


**Fig.3** Flag-shaped hysteresis model of SMA **Fig.4** Basic stress-strain responses of SMA wire with SE



 

## 3. Cyclic behavior of individual SMA cables

### 3.1 Material

The SMA considered in this study is composed of 50.8at.% nickel and 49.2at.% titanium. The SMA cables are produced from monofilament wires, which exhibit satisfactory superelasticity (SE) at room temperature [14]. Fig. 4 shows the typical flag-shaped stress-strain curve of the SMA monofilament wire, where satisfactory recoverability could be observed. In the loading path, a transformation-induced plateau is obviously seen when the austenite-martensite transformation start stress $\sigma_{Ms}$ is exceeded. With increasing strain, the alloy completely transforms from austenite to detwinned martensite at the transformation finish stress $\sigma_{Mf}$. Unloading is a process of reverse phase transformation, where the material experiences the martensite-austenite transformation start stress $\sigma_{As}$ and finish stress $\sigma_{Af}$ successively, and finally returns to the original point with limited residual strain. The excellent corrosion resistance of NiTi-SMA makes it suitable for use under high chloride environments, where offshore structures locate.

### 3.2. Cable specimens and test setup

In this study, the SMA cables with 7×7×0.8 (unit in mm) constructions were used, i.e., each cable consists of seven strands and each strand is composed of 7 wires with 0.8 mm diameter. Five specimens were examined, where the test codes and their main parameters are summarized in Table. 1. The main variable parameters were end grip type and free length. Two types of end grip (Fig. 5(a)), namely, epoxy resin end and screw bar end, were produced to prevent the cables from unraveling. In particular, the screw bar end was designed for convenient installation in practical application. The free length of the SMA cables refers to the distance between two inner edges of the grip ends, where 180mm and 240mm were considered here.

An MTS universal test machine with a load capacity of 250 kN was employed to apply the uniaxial load on the SMA cable specimens, as shown in Fig. 5(b). The top and the bottom hydraulic wedge grips tightly clamped both ends of the cable. Two loading protocols, namely, cyclic loading with incremental amplitudes and single constant loading, were considered. For the former case, the global strain $\varepsilon_o$ increased from 1% to 10% with an interval of 1% and each strain level was repeated twice. For the latter case, a global strain $\varepsilon_o$ of 20% was exerted for a single cycle. The average stress of the SMA cable can be obtained by dividing the cable force by the sum of the area of all the monofilament wires, and the global strain $\varepsilon_o$ was calculated by dividing the axial elongation by the corresponding free length of the SMA cable.

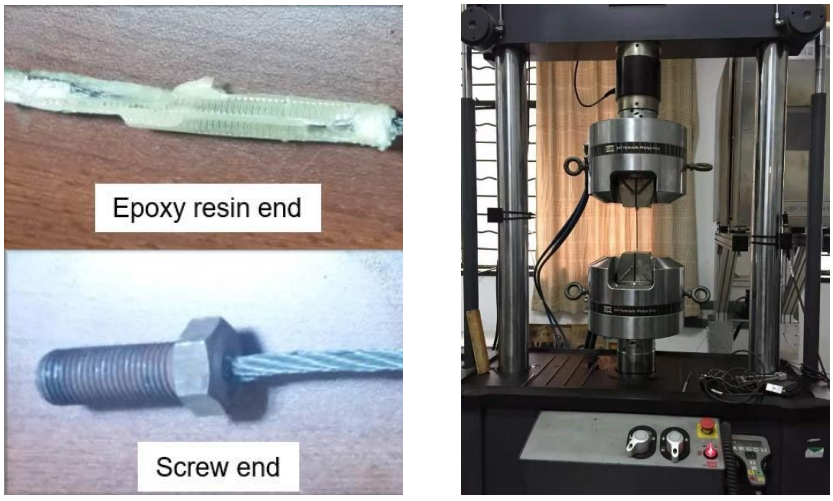


(a) (b)

**Fig.5** Details of SMA cable specimen and test setup



 

**Table 1** Testing parameters for individual SMA cables

| Test code | End socket type | Effective length (mm) | Construction | Monofilament diameter(mm) | Cross-sectional area ($mm^2$) | Loading type |
|---|---|---|---|---|---|---|
| 7×7×180S-I | Screw bar | 180 | 7×7 | 0.8 | 24.63 | Incremental cyclic loading |
| 7×7×240S-I | Screw bar | 240 | 7×7 | 0.8 | 24.63 | Incremental cyclic loading |
| 7×7×180R-I | Epoxy resin | 180 | 7×7 | 0.8 | 24.63 | Incremental cyclic loading |
| 7×7×180S-S | Screw bar | 180 | 7×7 | 0.8 | 24.63 | Single constant cycle |
| 7×7×180R-S | Epoxy resin | 180 | 7×7 | 0.8 | 24.63 | Single constant cycle |

## 3.3. Test results and discussion

### 3.3.1. Strength and stiffness

Fig. 6(a) (b) show the stress-strain curves of cable specimens 7×7×180S-I, 7×7×240S-I and 7×7-180R-I. As the number of cycles increases, the peak stress follows a rising trend, but certain degradation can be observed. The degradation phenomenon can be attributed to cable relaxation and transformation-induced fatigue (TIF) of virgin superelastic SMA[13]. The former is common for conventional cables, whereas the latter is a unique behavior of SMA material. It is difficult to quantify the exact proportion of the influence of the two factors, but the degradation effect can be effectively minimized by an appropriate “pre-exercising”.

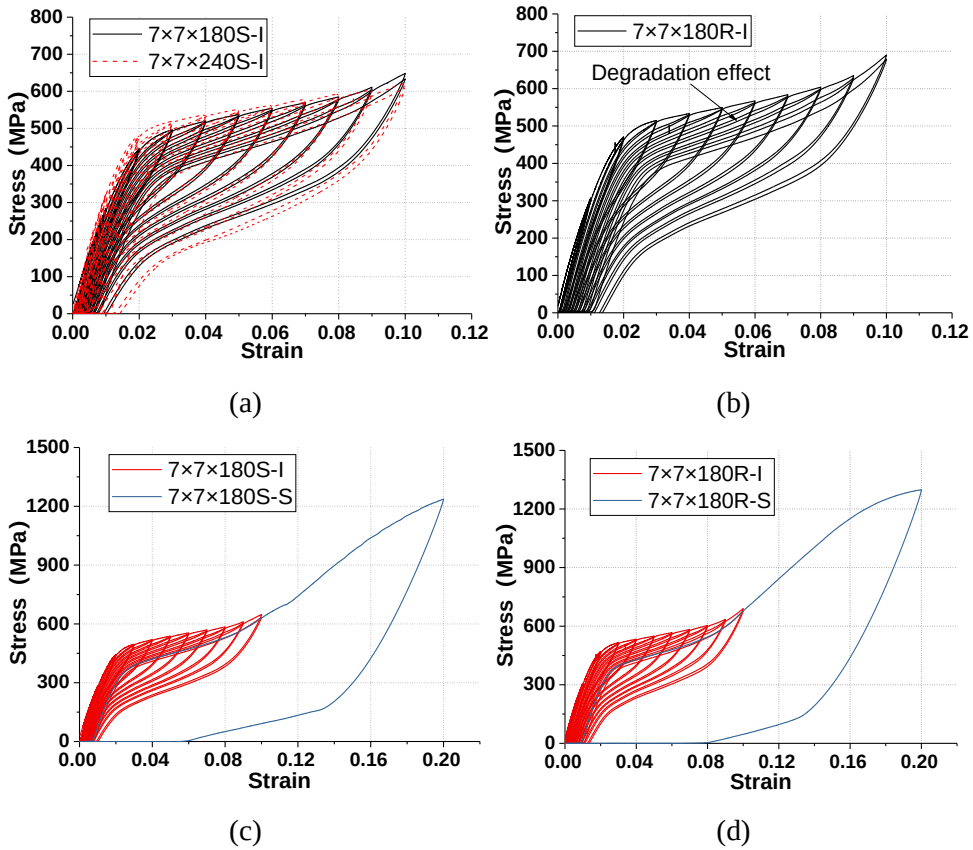


**Fig.6** Hysteretic behavior of SMA cables specimens



 

It is obvious that the specimens with different free lengths and end grips do not exhibit an obvious difference in the stress-strain response. For the specimens with the two kinds of loading protocols (shown in Fig. 6(c) (d) ), the skeleton curves are similar. This property is essential for the seismic application of the SMA cables (e.g., restrainers for bridges) because a reliable load-carrying capacity under unknown types of loading is desired. Also, an evident residual strain is induced for the specimens experiencing a peak strain of 20%, a case which is attributed to the actual yielding of the material. Based on the limited test data, 10% strain can be considered as a conservative threshold for the practical application of SMA cables.

Fig. 7(a) shows the variation trend of the yield strength of the SMA cable specimens. The yield strength could be roughly defined as the intersection of the two tangent lines along the initial elastic range and transformation plateau paths, as explained in the figure. In general, the yield strength shows a slight downward trend mainly due to the degradation effect[14]. Similar to the yield strength, the elastic modulus of each specimen decreases with an increasing number of loading (Fig. 7(b)).

### 3.3.2. Self-centering and energy dissipation capability

As shown in Fig. 7(c), residual strain accumulates with increasing loading cycles, although the value is limited. For instance, the maximum accumulated residual strain is below 1.1%, corresponding to a recoverable rate, i.e., the proportion of the restored strain to the achieved maximum strain, of more than 89%, after 20 cycles. It can be observed that the value of residual strain at the second cycle of the same loading amplitude is the same as that of the first cycle, which implies that the residual strain would stabilize if no new maximum strain arrives. Such a conclusion can also be confirmed from the previous investigation[14], and it highlights the necessity of pre-training SMA cables for practical application if obvious residual strain is not wanted.

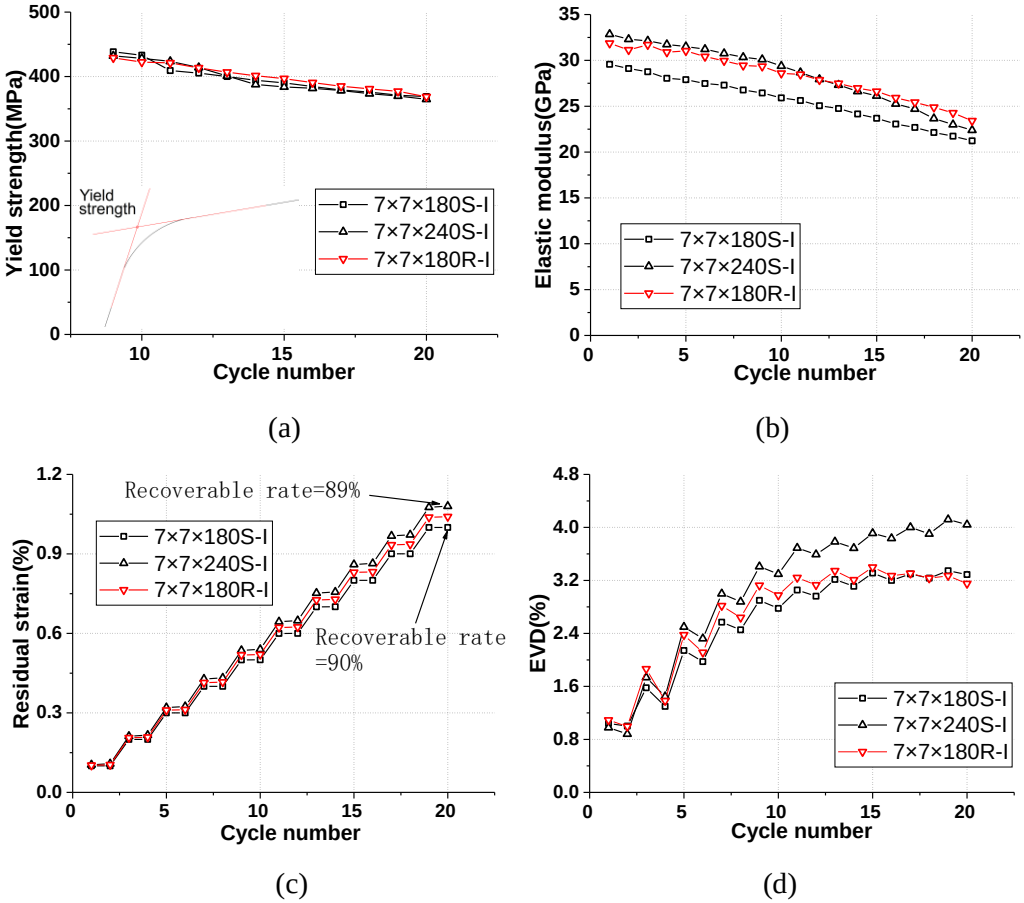


**Fig.7** Properties of SMA cable specimens: (a) yield strength (b) elastic modulus (c) residual strain (d) EVD



 

In addition to the expected self-centering capability, certain energy dissipation capacity is also one of the advantages of SMA cables. A dimensionless index, namely, equivalent viscous damping (EVD), is often introduced to quantitatively indicate the energy dissipation capacity, as expressed by:

$$EVD = \frac{W_D}{4\pi W_E} \tag{18}$$

where $W_D$ denotes the energy dissipation within a closed hysteretic loop. i.e., the total area of a given cycle; $W_E$ denotes the elastic energy accumulated along a linear stress-strain response with the same maximum value of displacement as that of the nonlinear system. As shown in Fig. 7(d), a maximum EVD of 4.0% is observed. The EVD typically increases obviously in the first few loading cycles and becomes stabilized in the last few cycles, which can be explained by an obvious rising of the peak point of the hysteretic loop but no significant change in the total hysteretic loop area (see Eq. (18)).

## 4. Case study

### 4.1. Bridge description and modeling

To evaluate the seismic mitigation efficiency of the proposed SMA-PF bearing, a typical simply supported RC box-girder bridge was selected for dynamic analysis. As shown in Fig. 8, the RC bridge has three spans, where the side span and the middle span are 20m and 30m, respectively. The width of the RC box-girder deck is 12.5m. Double-column bridge piers are adopted in the mid-span, and the size of the column is 8m (height) × 1.2m (diameter). The compressive strengths of unconfined concrete and confined concrete are 40.0 and 50.0 MPa, respectively. In addition, the yield strength ($F_y$) of the reinforcement is 440.0MPa, and the longitudinal and transverse reinforcement ratios are 1.35% and 0.2%, respectively. The in-span expansion joint considering the temperature effect is set to be 100mm. The detailed information about the PF and SMA-PF bearing is summarized in Table.2. The friction coefficient of the basic PF bearing is assumed to be 0.06[15]. The total area of the SMA cables was determined such that the total restraining force of the SMA cables at 10% strain accounts for 35% of the vertical load applied by the superstructure. The basic property of the SMA cables is illustrated in Fig. 9. The damping ratio of the bridge is assumed to be 5%.

**Table 2** Testing parameters for PF and SMA-PF bearing

| Parameters | Friction coefficient(μ) | Vertical load per bearing (KN) (side/middle span) | Initial slack(mm) | Total area($mm^2$) of SMA cables |
|---|---|---|---|---|
| PF bearing | 0.06 | 868/1362 | / | / |
| SMA-PF bearing | 0.06 | 868/1362 | 100 | 1103 |

A 3D finite element (FE) model of the RC bridge was generated in OpenSees [16] and the modeling details are shown in Fig. 8. Elastic beam-column elements were utilized to model the RC box-girder decks and pier caps since they typically remain elastic under strong ground motion. Mass was lumped into the corresponding nodes along the centerline. Fiber-type displacement-based beam-column elements were adopted to model the piers due to their possible nonlinear response. The piers were connected to the caps and footings using rigid link elements. Linear translational and rotational springs were used to model the pile foundations. The horizontal response of the SMA-PF bearing was simulated by the combination of elastic perfectly plastic and impact elements, and the vertical response was modeled using a linearly elastic element. The side abutments modeled. This study mainly focuses on the bridge response in the longitudinal direction,



 

which has been confirmed to control the response of the bridge [17]. In the meantime, the shear keys, which are usually utilized for controlling the transverse vibration of the bridge, are not considered here.

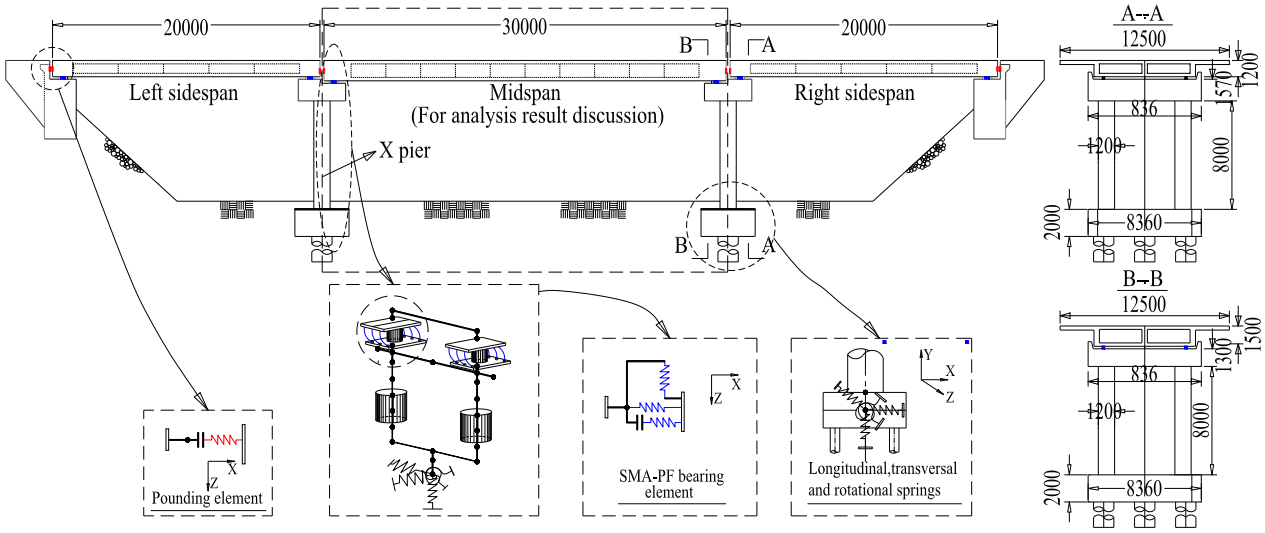


**Fig.8** Configuration of RC bridge and schematic illustration of bridge model

## 4.2. Selection of ground motions

It has been widely recognized that near-fault (NF) ground motions have special characteristics such as large-amplitude velocity pulses and large peak ground acceleration (PGA) and velocity (PGV)[18]. Many studies have investigated the seismic performance of bridge structures under near-fault ground motions and confirmed that more damages are induced in NF regions due to the high input energy[19].

A design response spectrum constructed for a site in southwest California, assuming soft rock conditions, is selected as the target spectrum. As shown in Fig. 10, three unscaled NF earthquake records are selected for response history analysis[20], with details listed in Table. 3.

**Table 3** Description of ground motions used in the analyses

| Earthquake name | Magnitude | Epicentral distance(km) | PGA(g) | PGV(m/s) |
|---|---|---|---|---|
| Northridge | 6.69 | 1.74 | 0.843 | 1.29 |
| Tabas | 6.19 | 7.35 | 0.854 | 0.99 |
| Landers | 7.28 | 2.19 | 0.72 | 1.33 |

## 4.3. Discussion of analysis result

An internal span is taken as an example for discussion. Two seismic response indicators, i.e. unseating displacement of girder deck and pier curvature ductility, are considered. The former refers to the relative displacement between the deck and abutment, and the latter is typically defined as the actual curvature divided by the yield curvature. Fig. 11 shows the monotonic moment-curvature response of the pier, from which the yield curvature could be obtained.

The typical force-displacement response (Tabas) of the PF and SMA-PF bearing are presented in Fig. 12. For the PF bearing, the load resistance provided by the friction force is constant, and the bearing displacement is not controlled. On the other hand, satisfactory restraining effect of the supplemental SMA cables could be observed.



 

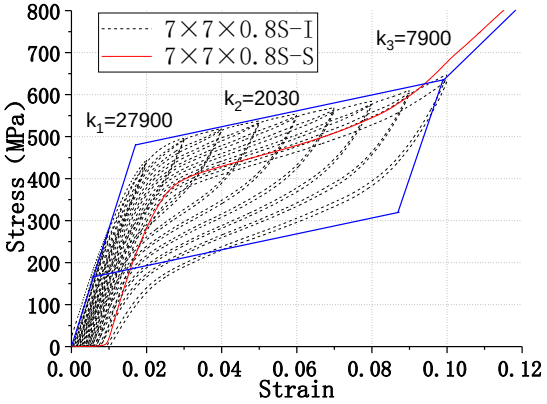


**Fig.9** Flag-shaped hysteresis model of SMA

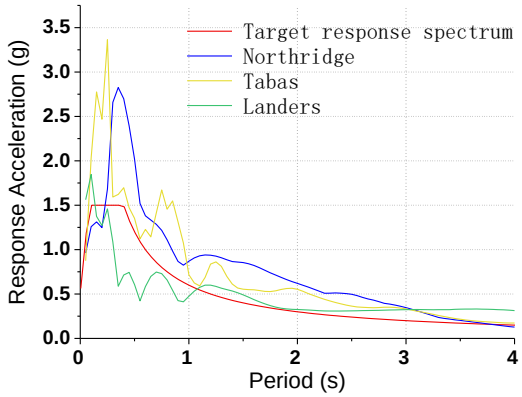


**Fig.10** Response spectra of selected ground motions

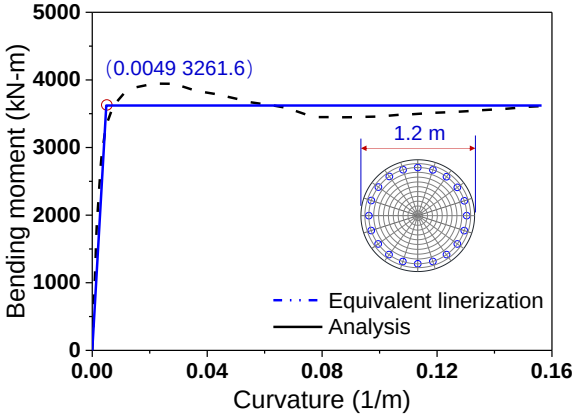


**Fig.11** Moment-curvature response of the pier

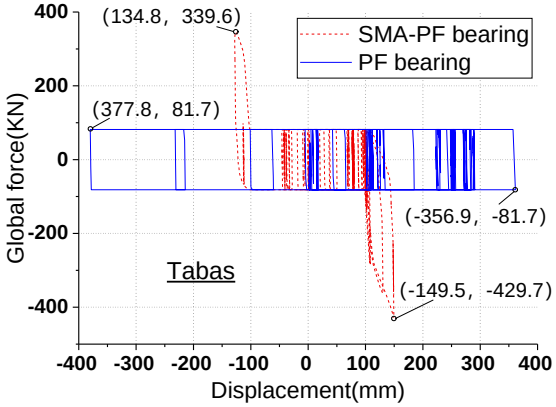


**Fig.12** Typical response of PF and SMA-PF bearings

As shown in Fig. 13, the deck isolated by the PF bearing slides for a large distance under pulse excitation, in which case the bearings would have been seriously damaged or even failed at such a large displacement. Moreover, the residual displacement of the PF bearing is often large (e.g., Fig. 13(c)), which would cause maintenance difficulties after the earthquake. On the contrary, the application of the SMA-PF bearing limits the residual displacement within a relatively narrow range. The SMA-PF bearing also shows its superiority in peak displacement control especially when the relative displacement exceeds the initial slack. Although not considered in this study, the expected displacement can be adjusted by changing the initial slack or total area of the SMA cables. One phenomenon that cannot be ignored is that the maximum unseating displacement of the SMA-PF bearing could occur in the reversed peak immediately after the major pulse ((Fig. 13(a) (b))), and this may be caused by the restoring force of the SMA cables. In any case, the maximum displacement in the reverse direction still stays at a controllable level. The maximum unseating displacement that the SMA-PF bearing experiences is 192.64 mm, corresponds to the maximum SMA cable strain of 19.2%.

As shown in Fig. 14, the introduction of the SMA cables slightly increases the curvature ductility demand. This phenomenon is expected as the involvement of the restraining force inevitably transmits the inertia force to substructure. However, due to the low stiffness at the transformation plateau and certain energy dissipation capability, the SMA cables have better buffering property compared with other conventional restrainers such as steel and FRP cables[21]. Considering the possible shock to the substructure, the total area of the SMA cables used in SMA-PF bearings need to be optimized, which is, however, beyond the scope of this study. Being consistent with the unseating displacement, the curvature ductility also achieves its maximum value in the reversed peak (Fig. 7(a)(b)).



 

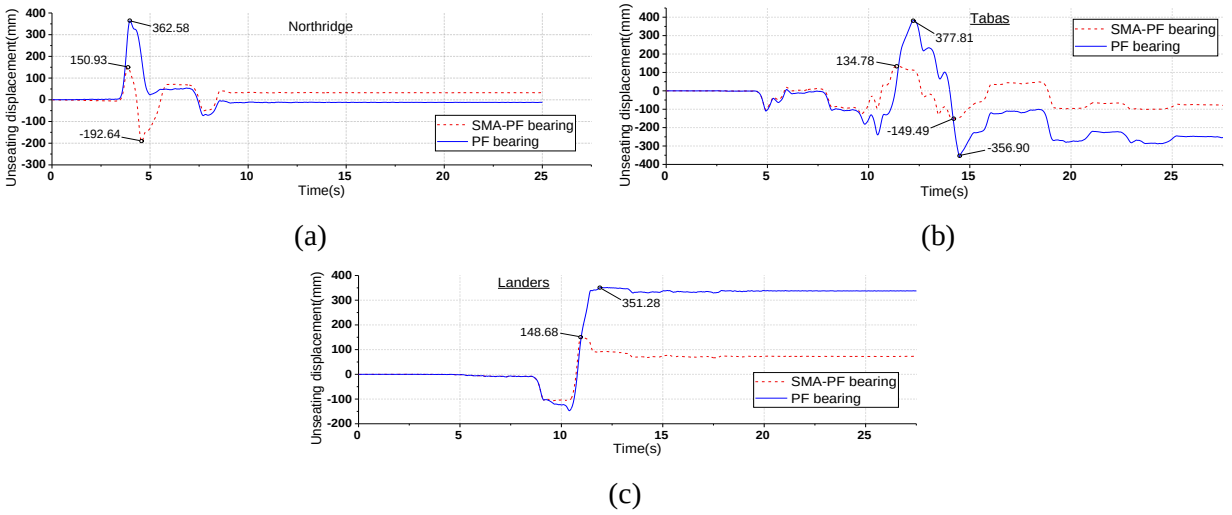


**Fig. 13** Time histories of unseating displacement of bridge isolated by PF or SMA-PF bearings

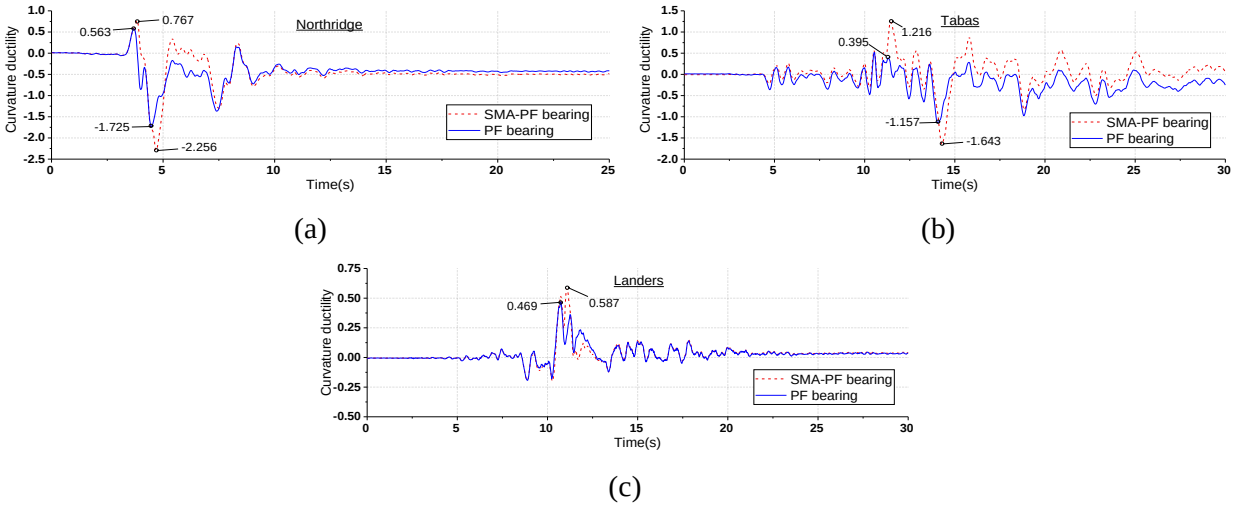


**Fig. 14** Time histories of pier curvature ductility of bridge isolated by PF or SMA-PF bearings

## 5. Conclusion

A new type of SMA-cable-based PF bearing system was proposed in this paper. The fundamental mechanical behavior of individual SMA cables was first studied, and subsequently a numerical case study on three-span simply supported bridges equipped with PF bearing and SMA-PF bearings was conducted. The study leads to the following observations and conclusions:

- Typical flag-shaped responses were observed for the SMA cable specimens under cyclic loading. The skeleton curves were similar for the specimens under cyclic incremental loading and single constant loading, which indicated that the loading types did not have an obvious influence on the property of SMA cables.
- The individual SMA cable specimens exhibited a satisfactory self-centering capability, e.g. the recovery rate is more than 89% when reaching a maximum strain of 10%. The residual strain became obvious after experiencing 20% strain. A 10% strain limit is recommended for the practical design of SMA cables, although the value may be refined following further investigations.
- The EVD of the SMA cable specimens at 10% strain ranges between 3.2% and 4%. The moderate energy dissipation capacity and the large recoverable strain range make the SMA cables ideal candidates



 

for passive structure control.

- The case study on a model bridge confirmed that the SMA-PF bearing encourages enhanced displacement control capability at the cost of a minor increase in the load transmitted to the piers. The curvature ductility of the piers in the bridges with the SMA-PF bearings is still maintained at controlled levels.

## 6. Acknowledgements

The financial support from the National Natural Science Foundation of China (NSFC) with Grant Nos. 51778456 and 51978513 is gratefully acknowledged. Support is also provided by the Shock and Vibration of Engineering Materials and Structures Key Laboratory of Sichuan Province (18kfgk05).

## 7. References

[1] M. Dolce, D. Cardone, and G. Palermo, "Seismic isolation of bridges using isolation systems based on flat sliding bearings," *Bulletin of Earthquake Engineering*, vol. 5, no. 4. pp. 491–509, 2007.
[2] Y. T. Hsu and C. C. Fu, "Seismic effect on highway bridges in Chi Chi earthquake," *J. Perform. Constr. Facil.*, vol. 17, no. 2, pp. 47–53, 2003.
[3] A. Ghobarah and H. M. Ali, "Seismic performance of highway bridges," *Engineering Structures*, vol. 10, no. 3. pp. 157–166, 1988.
[4] M. Dicleli and M. Bruneau, "Seismic performance of multispan simply supported slab-on-girder steel highway bridges," *Eng. Struct.*, vol. 17, no. 1, pp. 4–14, 1995.
[5] H. Zargar, K. L. Ryan, and J. D. Marshall, "Feasibility study of a gap damper to control seismic isolator displacements in extreme earthquakes," *Struct. Control Heal. Monit.*, vol. 20, no. 8, pp. 1159–1175, 2013.
[6] G. Reginald DesRoches, "Design of seismic cable hinge restrainers for bridges," *J. Sound Vib.*, vol. 126, no. 4, pp. 500–509, 2000.
[7] R. DesRoches, T. Pfeifer, R. T. Leon, and T. Lam, "Full-scale tests of seismic cable restrainer retrofits for simply supported bridges," *J. Bridg. Eng.*, vol. 8, no. 4, pp. 191–198, 2003.
[8] J. Wang, S. Li, F. Hedayati Dezfuli, and M. S. Alam, "Sensitivity analysis and multi-criteria optimization of SMA cable restrainers for longitudinal seismic protection of isolated simply supported highway bridges," *Eng. Struct.*, vol. 189, pp. 509–522, 2019.
[9] B. Shrestha, H. Hao, and K. Bi, "Devices for protecting bridge superstructure from pounding and unseating damages: an overview," *Struct. Infrastruct. Eng.*, vol. 13, no. 3, pp. 313–330, 2016.
[10] C. Fang, M. C. H. Yam, T.-M. Chan, W. Wang, X. Yang, and X. Lin, "A study of hybrid self-centring connections equipped with shape memory alloy washers and bolts," *Eng. Struct.*, vol. 164, pp. 155–168, 2018.
[11] C. Fang *et al.*, "Application of an Innovative SMA Ring Spring System for Self-Centering Steel Frames Subject to Seismic Conditions," *J. Struct. Eng.*, vol. 144, no. 8, 2018.
[12] W. Wang. Cheng Fang, *Shape memory alloys: modeling and engineering applications*. Nature Singapore: Springer Nature Singapore, 2020.
[13] B. Reedlunn, S. Daly, and J. Shaw, "Superelastic shape memory alloy cables: Part I – Isothermal tension experiments," *Int. J. Solids Struct.*, vol. 50, no. 20–21, pp. 3009–3026, 2013.
[14] C. Fang, Y. Zheng, J. Chen, M. C. H. Yam, and W. Wang, "Superelastic NiTi SMA cables: Thermal-mechanical behavior, hysteretic modelling and seismic application," *Eng. Struct.*, vol. 183, pp. 533–549, 2019.
[15] "Seismic Design Criteria Version 1 . 3," *Foundations*, no. February, 2004.
[16] S. M. McKenna F, Fenves GL, "Open system for earthquake engineering simulation (OpenSees)," *Berkeley, CA: University of California*, 2000.
[17] E. Choi, R. DesRoches, and B. Nielson, "Seismic fragility of typical bridges in moderate seismic zones," *Eng. Struct.*, vol. 26, no. 2, pp. 187–199, 2004.
[18] R. S. J. P. Bhasker Rao, "Performance of sliding systems under near-fault motions," *Nucl. Eng. Des.*, 2001.
[19] S. Jangid and J. M. K. R., "Base isolation for near-fault motions," *Earthq. Eng. Struct. Dyn.*, 2001.
[20] PEER (Pacific Earthquake Engineering Research Center), PEER Ground Motion Database, University of California, Berkeley, CA, 2013. http://ngawest2.berkeley.edu/.
[21] S. Li, F. Hedayati Dezfuli, J.-Q. Wang, and M. S. Alam, "Displacement-Based Seismic Design of Steel, FRP, and SMA Cable Restrainers for Isolated Simply Supported Bridges," *J. Bridg. Eng.*, vol. 23, no. 6, 2018.



 